

***In situ* photoelectron spectroscopy investigation of silicon cluster growth on fullerene surfaces**

P. Reinke

Department of Materials Science and Engineering, University of Virginia, Charlottesville, Virginia 22903, USA

P. Oelhafen

Institut für Physik, Universität Basel, Klingelbergstrasse 82, 4056 Basel, Switzerland

(Received 3 September 2004; published 18 January 2005)

The growth of Si clusters on the C_{60} surface was observed *in situ* using photoelectron spectroscopy in the ultraviolet (UPS) and x-ray regimes. The highly corrugated C_{60} surface provides a wide range of bonding sites and might function as a template for the formation of cluster superstructures. The Si accumulates first in the interstitial bonding sites, which present a bonding environment defined by the fullerene molecules and dominated by carbon atoms. This arrangement is comparable to the formation of a surface fulleride and the interstitial sites apparently act as primary nucleation sites. The clusters then continue to grow and the Si—Si bonding environment gains in importance. A numerical fit of the core level spectra ($C1s$ and $Si2p$) reveals the relative contributions of the different bonding environments as the cluster growth proceeds. The absence of a SiC contribution excludes a substitutional doping of the fullerene cage with Si. The impact of initial and final state effects due to changes in the photoemission process as the cluster size is varied, can be identified and separated from the influence of the chemical shift (variation in bonding environment) on the core level position and shape. The UPS valence band spectra confirm the absence of a charge transfer or directed covalent bonding between the Si adsorbate and the fullerene surface. The valence band offset between the amorphous Si and the C_{60} amounts to 1.2 eV, and the position of the $C1s$ core level is likely pinned by the α -Si dangling bonds. The C_{60} can function as a template for the formation of Si cluster arrays (superstructures) with the interstitial sites as primary nucleation sites and an expansion to three-dimensional structures is possible.

DOI: 10.1103/PhysRevB.71.045420

PACS number(s): 81.07.Nb, 71.20.Tx, 79.60.Jv

INTRODUCTION

Fullerenes are covalently bonded spherical carbon clusters which assemble to extended van der Waals bonded solids and are recognized as the third carbon allotrope, in addition to diamond and graphite.¹ The pristine material possesses interesting properties but the addition of foreign elements as dopants can lead to a considerable expansion in the variability of properties.^{2–4} Different doping pathways exist and include endohedral doping where the foreign atom is located inside the cage, substitutional doping where a carbon atom in the cage wall is substituted, and exohedral doping. In exohedral doping the foreign element occupies the relatively large vacancies in between the fullerene molecules. Several atoms can be inserted and form clusters with up to 11 atoms ($Na_{11}C_{60}$).⁵ Exohedral doping and thus the formation of fullerides can lead to the formation of novel materials with quite surprising properties, such as the superconducting K_3C_{60} .⁶ Fullerides are per definition exohedrally doped fullerenes in the crystalline phase, the term surface fullerides is also used in the study of the accumulation of foreign elements on the fullerene surface. Since the crystallinity and long-range order in our materials can often not be confirmed we decided to introduce the term composite material for the three-dimensional (3D) material (thin layers) or surface clusters for the 2D material (deposition of dopant on the C_{60} surface).⁷

The thermodynamic stability of fullerides has been considered^{2,4} using a Born-Haber cycle and it was concluded in this study that ionic fullerides with alkalis and some earth

alkalis^{8,9} are indeed thermodynamically stable. The stability of other types of fullerides which might include covalent rather than ionic bonding, is still being discussed but the relatively large cohesive energy of many metals might prevent formation of fullerides by a solid state process. It has, on the other hand, been shown that the codeposition of both reactants from the gas phase can lead to the formation of fulleridelike phases. The formation of Ti, Yb, and Nb fullerides^{10–13} has been achieved by rapid condensation of the reactants from the gas phase. This kinetically controlled deposition process allows one to synthesize a much broader range of fullerides and C_{60} /metal composite materials which do not undergo a spontaneous segregation and are most likely metastable.

The combination of fullerenes with Si has been suggested as a pathway to stabilize the C_{60} network, but is also of interest for the formation of contacts and the building of Si nanonetworks embedded in a C_{60} matrix.^{14–19} The synthesis of 3D C_{60} -Si composites has been described in an earlier publication¹⁸ and in order to gain an improved understanding of the interaction of Si atoms with the C_{60} surface the present study concentrates on the 2D system, the deposition of Si on a C_{60} surface. These results might also be of interest in the application and contacting of carbon nanotubes.

Various aspects of the interaction of Si with fullerenes have been discussed in the literature and the most common experiment is the deposition of C_{60} on a Si surface.^{20–25} The type of bonding at the interface has been reported to depend on the Si surface termination (hydrogen saturation, type of reconstruction, and orientation), on the surface coverage with fullerenes and the temperature. The doping of C_{60} with Si

has also been suggested¹⁹ as a method to stabilize C_{60} layers and thus expand the range of applications by the introduction of an element which is not purely van der Waals bonded. An interesting prediction has been made by Marcos *et al.*¹⁶ for the formation and bonding of Si clusters with 1 to 15 atoms in contact with C_{60} . In the framework of a tight binding study they find that Si_n clusters/aggregates prefer the contact with the C_{60} for $n < 5$ but if n is larger the formation of three-dimensional Si clusters is preferred. This also indicates that the C_{60} surface might serve as a template for the growth of ultrasmall Si clusters¹⁴ if the interstitials between the molecules are preferred nucleation sites. The study we present here focuses on observing the progression of Si overlayer growth on a C_{60} surface with photoelectron spectroscopy (PS) in the x-ray (XPS) and ultraviolet regime (UPS). PS is sensitive to the local environment of the atoms and yields information on the electronic structure at the interface and the progression of the Si growth at the surface. In combination with a numerical fit procedure it is possible to separate different bonding states of the Si atoms and develop a concise description of the cluster growth.

EXPERIMENTAL

In a first step the C_{60} layer was deposited on a Si(100) substrate (room temperature) up to a final film thickness of 20 nm at a deposition rate of 0.3 nm/min. The C_{60} beam was created with a sublimation source that consists of a tantalum sleeve attached to a simple button heater and is loaded with commercially available C_{60} . Careful outgassing of the material resulted in a highly stable deposition rate. The silicon atom beam was produced by electron beam evaporation of silicon and a deposition rate of 0.08 nm/min was used. Si layers which are deposited on samples held at room temperature have an amorphous microstructure and recrystallization occurs only upon heating to more than 800 °C. The deposition rates were monitored by a quartz crystal monitor and calibrated by separate deposition of a pure C_{60} or *a*-Si layers and measuring the resultant film thickness. A good agreement was found between the measured film thickness and the expected value calculated for the frequency change of the quartz crystal monitor taking into account the mechanical properties of an *a*-Si layer.

The nominal coverage is the film thickness which would be reached if the film growth proceeds in a layer-by-layer growth mode. All the depositions were performed under ultra high vacuum conditions with a base pressure below 10^{-10} mbar and the sample is transported to the analysis chamber without breaking the vacuum. The only contaminant in the films were traces of oxygen, with a maximum concentration of 1 at. % at the end of the experiment.

The photoelectron spectroscopy analysis was performed with a Leybold-SPECS EA11/100 MCD (multichannel detection) spectrometer. Monochromatized AlK_{α} ($h\nu = 1486.6$ eV) radiation was used to record the core level spectra (MXPS), and a helium gas discharge lamp emitting light in the ultraviolet region (UPS, He I, $h\nu = 21.22$ eV, He II, $h\nu = 40.82$ eV) was employed to record the valence band (VB) spectra. The typical resolution is 0.6 eV for the

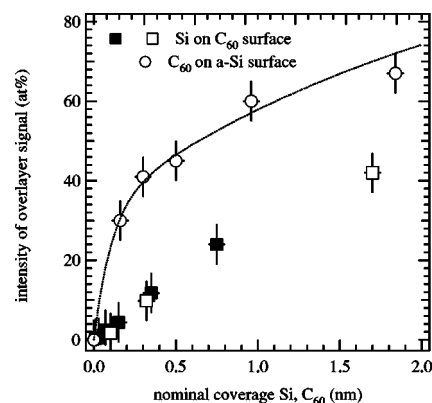


FIG. 1. Intensity of the overlayer signal ($Si2p$ for *a*-Si on C_{60} , $C1s$ for C_{60} on *a*-Si) as a function of the nominal coverage. In the deposition of C_{60} on *a*-Si (open circles) the graph can be described using the Lambert-Beer law and is therefore in agreement with a layer-by-layer growth (electron mean free path of 1.6 nm). The dotted line serves as guidance for the eye. The deposition of Si on the C_{60} surface includes two sets of data, indicated by the black and open square markers.

MXPS spectra and about 0.1–0.2 eV for the UPS measurements. The core level spectra were recorded using a constant pass energy, while for the VB spectra a constant retardation ratio was used. The spectra are presented without satellite subtraction and the energies are referenced to the Fermi level and the $Au 4f_{7/2}$ line (positioned at 84.0 eV) of a clean gold sample. The element concentrations are calculated using the photoexcitation cross sections by Yeh.²⁶ None of the films exhibited any charging during the photoelectron spectroscopy analysis; due to their small thickness the loss of charge by photoelectrons emitted at the surface can be equilibrated by photoelectrons injected into the layer from the underlying substrate.

The numerical fit procedure used for the analysis of the core level peaks follows the procedure for a least square fit developed by Marquard.²⁷ The peak shape is described with a Doniach-Sunic function²⁸ and a Shirley background.²⁹ The core level peaks for the pure materials, amorphous Si and C_{60} , are included in the figures. The quality of the fit is judged by considering the residuals, it was possible in all cases to isolate a best fit result and using either more or fewer peaks lead to a considerably worse agreement with the experimental peak shape. The best results which were obtained in the fit procedure for the $Si2p$ core level are included in the figures.

RESULTS

Figure 1 illustrates the changes in the intensity of the overlayer signal as a function of the nominal coverage for two different experiments: the deposition of Si on a C_{60} surface, and the inverted experiment, the deposition of C_{60} on an *a*-Si surface. The function which describes the change in intensity of the overlayer signal is determined by the growth mode, and in the case of a layer-by-layer growth an exponential function given by the Lambert-Beer law can be used.

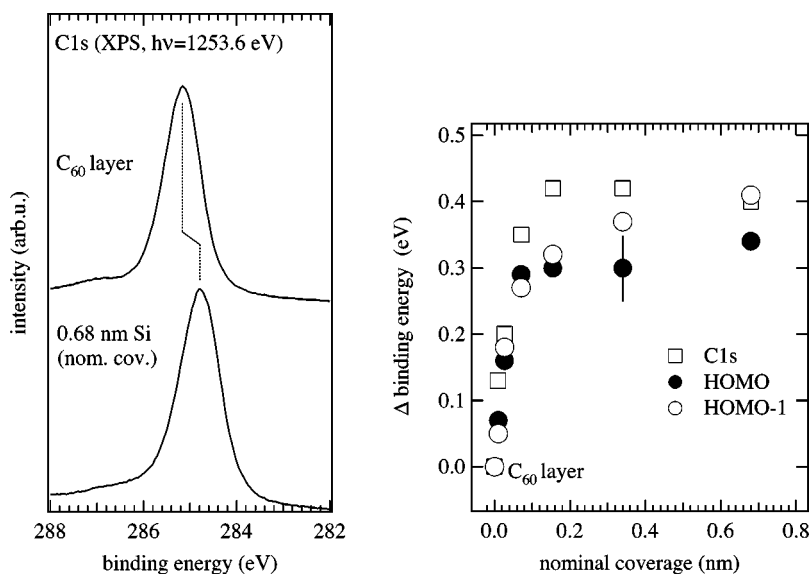


FIG. 2. Left-hand side: Carbon 1s core level peak for the C₆₀ surface and after the deposition of 0.68 nm Si. Right-hand side: Change in the position of the carbon 1s peak (from XPS spectra), highest occupied molecular orbital (HOMO) and HOMO-1 (from UPS spectra) as a function of nominal Si coverage. The reference value (Δ binding energy=0) is taken from the clean C₆₀ surface: C1s: 285.1 eV, HOMO: 2.45 eV, and HOMO-1: 3.78 eV. All peaks are shifted to smaller binding energies.

Knowledge of the mean free path of electrons in the solid is required to apply the Lambert-Beer law. The value of 1.6 nm for the C₆₀ overlayer was determined experimentally by annealing a thick C₆₀ layer (deposited on an *a*-Si surface) at 500 °C. This is well below the onset of carbide formation¹⁸ but above the sublimation temperature of C₆₀. Only a single monolayer of the fullerene molecules remains on the surface and the intensity of the Si can C signals can now be used to calculate the electron mean free path in C₆₀. This value is also in good agreement with the universal curve of the electron mean free path in solids.³⁰ The growth of C₆₀ on the *a*-Si surface closely follows a layer-by-layer growth as described by the Lambert-Beer law, while the growth of Si on the C₆₀ surface cannot be described with the exponential Lambert-Beer function using a reasonable value for the mean free path. Apparent deviations from the Lambert-Beer law can also occur if the sticking coefficient of the incoming particles is smaller than unity. The strength of the interaction between Si and C₆₀ is considerable^{31–34} and we can therefore assume that the sticking coefficient of Si-atoms is indeed close to unity. The observed intensity changes can consequently not be attributed to the desorption of Si atoms but are due to the growth of the Si overlayer via island or cluster formation.

The analysis of the C1s and Si2p core levels reveals a more detailed picture of the growth process and the interaction between Si and the C₆₀ surface. The C1s core level for the virgin C₆₀ surface and for a nominal Si coverage of 0.68 nm are shown in Fig. 2(a). The C1s peak of the C₆₀ surface is located at 285.1 eV and shifted to lower binding energies in the course of the Si deposition, which is illustrated in Fig. 2(b). The peak shift reaches its maximum value of 0.4 eV (284.7 eV) at a nominal coverage of 0.17 nm (not shown), no further changes are observed for higher coverages. Apart from the change in binding energy the peak parameters remain nearly constant, only a small increase in the full width at half maximum of 0.1 eV (from 0.6 to 0.7 eV) is observed. Covalently bonded SiC which would give rise to a peak at 283.2 eV,³⁵ is absent in all spectra and a substitutional doping where a Si atoms substitutes a C atom in the

fullerene cage, can therefore be excluded. Also included in Fig. 2(b) are the shifts of the highest occupied molecular orbital (HOMO) and HOMO-1 peak which are derived from the UPS spectra.^{31,32,36–39} The position of the HOMO peak prior to the addition of Si is at 2.45 eV and the HOMO-1 peak is located at 3.78 eV. A more detailed discussion of the UPS spectra is given later in the text.

The Si2p core level spectra are summarized in Fig. 3, where the Si2p core level is depicted as a function of Si coverage. The relatively poor signal to noise ratio in the first few spectra is due to the very low surface concentration of Si and its relatively small photoexcitation cross section. On the right-hand side of the figure three examples are included which serve to illustrate the results of the numerical fit procedure. Each Si2p core level consists of two contributions from the spin orbit splitting,³⁰ Si2p_{1/2} and Si2p_{3/2}, which appear at a constant energetic distance (0.6 eV) and have a constant branching ratio 2p_{3/2}/2p_{1/2} of 2.0. The results shown represent the best possible fit which could be achieved, an increase or decrease in the number of peaks worsened the agreement with the experimental data. The position of the high binding energy peak is at 101.3 eV at the beginning of the experiment, the low-binding energy components at 100.2 eV. Numerous effects which are described in the next paragraphs modify the binding energy of photoelectrons emitted from small clusters and a comparison with SiC (100.4 eV) is therefore meaningless for the Si2p peak.

In a visual inspection of the Si2p peak it is apparent that the peak shape undergoes considerable changes: while the first peak at very low Si coverage exhibits a shallower slope on the high binding energy side, commensurate with the presence of Si2p_{1/2} and Si2p_{3/2} contributions (see *a*-Si reference), the shallower slope appears on the low binding energy side as the deposition progresses. This is particularly obvious in the third deposition step (0.07 nm nominal coverage). This change in shape cannot be attributed to initial or final state effects which modify the photoemission process in small clusters (see next paragraph for details),³⁰ and the introduction of at least one additional component is required. The numerical fit was carried out using two components which

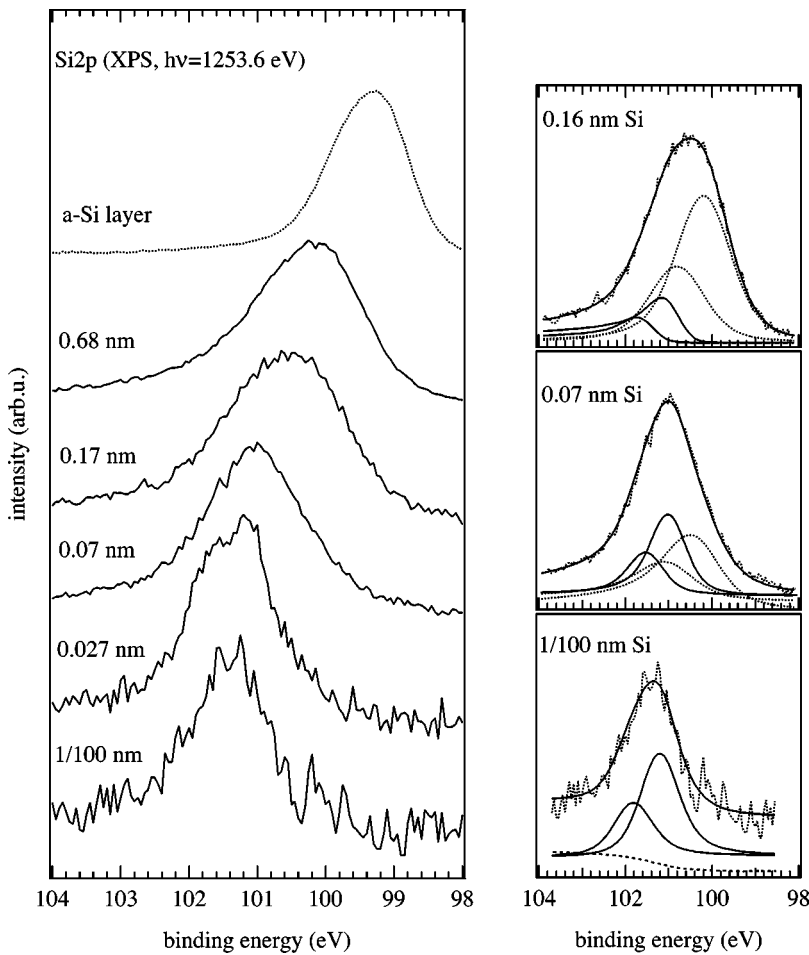


FIG. 3. On the left-hand side the Si2p core level spectra are shown as a function of nominal Si coverage. On the right-hand side three examples of the numerical fit procedure are included.

consistently yielded the best results. The visual inspection of the peak shape as a function of coverage already indicates a deviation from the assumption of a continuous cluster growth. Rather small variations in peak shape combined with a continuous shift to lower binding energy would be expected for a continuous cluster growth in the absence of different bonding sites at the surface. This has, for example, been observed for Au cluster deposition on a vitreous carbon substrate.⁴⁰

Two components contribute with varying intensity to the Si2p core level: a component at higher and lower binding energy can be distinguished. The high-binding energy component dominates at low coverage, while the low-binding energy component is more prominent at higher coverages. With increasing nominal coverage the low-binding energy component gains in intensity and its peak shape and position approach that of a-Si which is included at the top of Fig. 3. The positions of the two components are shown as a function of the nominal coverage in Fig. 4. The position of the Si2p peak maximum determined from the original core level peak prior to the numerical fit are also included. The contribution of the high-binding energy component to the Si2p peak decreases rapidly with coverage but the absolute height of this peak remains constant. It is overwhelmed by the rapid intensity increase in the low-binding energy component and hidden below this intense peak. The Si atoms which arrive at the surface now only contribute to the low-binding energy com-

ponent. At a nominal coverage around 0.15 nm the high-binding energy contribution to the Si2p peak drops below a few percent. It is a general observation made for different systems that if the contribution of a component to the main

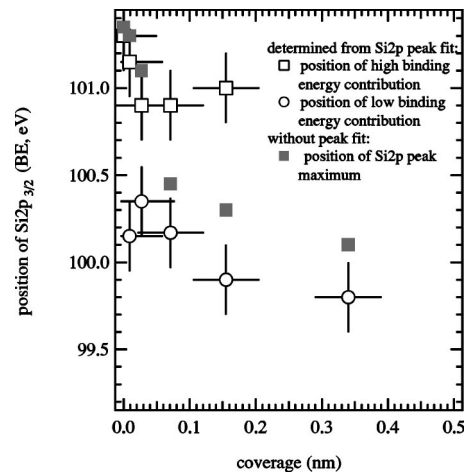


FIG. 4. This figure summarizes the results of the fit procedure and includes the position of the Si2p peak contributions at high binding energies (open squares) and the one at low binding energies (open circles). The grey filled squares show the position of the Si2p peak maximum obtained without a numerical fit.

peak drops below about 5% the fit procedure becomes unreliable.

The binding energy difference between the two components is labeled *A* and the continuous shift to lower binding energies is labeled *B*. The binding energy difference *A* is 0.9 ± 0.1 eV and the binding energy shift *B* is 0.4 eV at a nominal coverage of 0.34 nm, and 0.8 eV at 1.7 nm nominal coverage, where the bulk value for *a*-Si (99.4 ± 0.05 eV) is reached. The low-binding energy component is always broader and slightly more asymmetric than the high-binding energy component.

The photoelectron binding energy observed for small clusters is influenced by several effects which are connected to small size of the system.^{40–43} Initial state effects, the variation of the density of states with cluster size, and final state effects which stem from the delayed relaxation of the photohole, contribute to the dependence of the binding energy and VB structure on cluster size. The final state effects dominate the peak shift in metal clusters on semiconducting or insulating surfaces and are caused by a delay in the relaxation of the photohole as compared to the time scale of the photoelectron emission. If the cluster is still positively charged when the photoelectron is emitted an additional electrostatic barrier will reduce the electron kinetic energy (increase the apparent binding energy). The relaxation of the photohole depends on the cluster size (the cluster acts as a spherical capacitor and the relaxation time depends on $1/r$) and the efficiency of electron transfer from the substrate to the cluster. Both processes have a probability distribution in time which leads to a peak broadening. The presence of a variety of cluster sizes leads to an additional distortion and broadening of the peak shape. For Au clusters on amorphous carbon substrates the peak shift as a function of size has been quantified using size selected clusters,⁴⁰ and the delayed photohole relaxation has been shown to dominate. A peak shift is observed for clusters smaller than about 2.0 nm, and can be up to 1.0 eV for very small Au clusters (Au_5). It can in turn be used to assess cluster size distributions in equivalent systems. These numbers can unfortunately not be translated to the Si- C_{60} system mainly due to the lack of knowledge of the efficiency of electron transfer across the interface.

The observation of the change in peak shape and the results of the numerical fit procedure indicate the presence of at least two main determinants for the binding energy of the two components: a continuous shift to lower binding energies which is strongly dependent on the cluster size (respectively, the nominal Si coverage) and binding energy difference between the two components which remains constant as long as both components can be detected. The strong cluster size dependence of the binding energy shift indicates that the influence of initial and final state effects dominate. The magnitude of the various contributions cannot be determined unambiguously from the present experiment, although most other experiments indicate that the shift induced by the delayed core hole relaxation dominates.

In addition to the core levels the UPS valence band spectra were recorded for every deposition step and a selection of the spectra measured with HeI and HeII light as excitation source are included in Fig. 5. The VB spectrum of the pure C_{60} layer is dominated by a number of relatively narrow

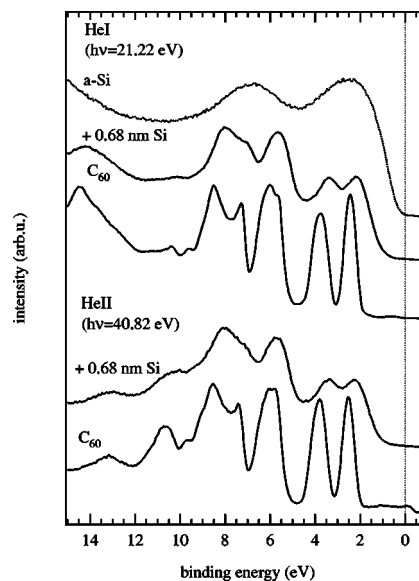


FIG. 5. Selection of UPS-valence band spectra for the clean C_{60} surface and for a nominal Si coverage of 0.68 nm. For comparison the VB spectrum of an *a*-Si layer is included at the top of the figure. In the *a*-Si spectrum the peak at 6.7 eV stems from Si oxides, the oxygen concentration was about 1% in this layer, but the excitation cross section for the oxides is considerably larger than for the *a*-Si-VB. All spectra are normalized to unit height.

peaks, which can be assigned to the bands formed by the occupied molecular orbitals (MOs) of C_{60} which have been described in numerous publications. A narrow peak is positioned at 2.42 eV (HeI) and 2.52 eV (HeII) and is due to excitation from the highest occupied MO (HOMO); the HOMOs have merged to form a fivefold-degenerate band of h_u symmetry.^{44–47} The VB-spectrum of an *a*-Si layer is included at the top of the figure; it is mostly featureless and dominated by a relatively broad peak centered at 2.2 eV, the valence band maximum is at 0.2 eV.

Moving from the pristine C_{60} surface to increasing Si coverage a shift of all C_{60} related features by 0.4 eV to lower binding energies is observed without variation of their relative position, this is commensurate with a rigid band behavior and indicates that no preferential interaction of one MO with the Si clusters exists. Suto *et al.*³³ have pointed out the appearance of additional peaks can be a signature of the chemisorption of C_{60} on a $\text{Si}(111)7 \times 7$ and a $\text{Si}(100)2 \times 1$ surface, but no such behavior can be observed here. The broadening of the C_{60} features is connected to a hybridization between the carbon and silicon orbitals, and the loss in symmetry through the introduction of an interface. The consequent loss of degeneracy in the C_{60} -MOs leads to the observed broadening. The region close to the Fermi energy is dominated by the states from the *a*-Si matrix, where the dangling bonds and band tail states contribute and form a diffuse background which tapers off to zero close to the Fermi energy. In the spectra of the pristine C_{60} surface two very small peaks are observed between the Fermi energy and the HOMO peak; these are associated with the emission of photoelectron excited by a satellite line emitted from the non-monochromatic He lamp. The evolution of the spectral shape

reflects an increasing contribution of *a*-Si. The spectra can be described by linear combination of the VB spectra of the pure materials after adjusting for the binding energy shifts. The very intense emission from the C₆₀ makes it difficult, if not impossible, to obtain information on the valence band structure of the Si clusters at the surface. To separate the Si contribution a variation of the photon energy or an enhancement of the surface sensitivity by using a shallow angle for photoelectron detection might yield in a future experiment information on the electronic structure of the clusters themselves. In agreement with the experiments reported for the absorption of C₆₀ on either crystalline or amorphous Si surfaces we did not observe an increase in the density of states and appearance of a new peak or steplike feature at the Fermi energy, which would be an indicator for a direct charge transfer to the LUMO (lowest unoccupied molecular orbital) of C₆₀.

The valence band offset is the energy difference between the valence band maxima (VBM) of the participating materials and determines the potential step at the interface of the completed *a*-Si-C₆₀ heterostructure and therefore strongly influences the electronic properties. If the positions of the VBM of both components are recognizable in the spectra the value of the offset can be directly determined by inspection. The *a*-Si VBM is indeed visible in the spectra since the contribution from C₆₀ in the region close to E_F is negligible, but only approximate values for the position of the VBM can be given for C₆₀ due to the superimposed *a*-Si features. Alternatively the valence band offset ΔE can be calculated with improved precision using the relation given in Ref. 48 from the positions of the core levels and valence band maxima of the pure and final heterostructure material:

$$\Delta E(C_{60}/a\text{-Si}) = (C1s_{C60} - \text{VBM}_{C60})_{\text{pure layer}} - (\text{Si}2p_{a\text{-Si}} - \text{VBM}_{a\text{-Si}})_{\text{pure layer}} - (C1s_{C60} - \text{Si}2p_{a\text{-Si}})_{\text{final}}.$$

The values are for the C1s peak: 285.1 eV for pure C₆₀ and 284.7 eV for the highest nominal coverage where no more changes in position of the core level are observed, and for the Si2p peak: 99.4 eV for *a*-Si and the *a*-Si overlayer at the end of the deposition experiment. The positions of the valence band maxima of the pure materials are 1.8 eV for C₆₀, and 0.2 eV for *a*-Si. The resultant valence band offset is 1.2 eV. This value is about twice the valence band offset reported by Janzen *et al.*²⁰ between a C₆₀ overlayer and a Si(111)7×7 surface. It has to be kept in mind that the *a*-Si electronic structure and the presence of a large amount of dangling bonds at the interface will lead to an electronically quite different behavior than the contact to a crystalline surface. The parallel shift of the C1s core level, the HOMO and HOMO-1 peaks (see Fig. 2) is commensurate with a band bending induced shift. The Fermi level is pinned by the increasing number of Si clusters and in particular the Si-dangling bonds at the interface. Please note that the values inserted in the calculation only include numbers deduced from the pristine materials and the final stage of the growth process where effects which are cluster size dependent can be excluded. The position of the Si2p core level for the *a*-Si layer on C₆₀ and a thick *a*-Si layer on a different sub-

strate are equivalent which means either the band bending is always the same or the *a*-Si layer does not support a significant electrostatic potential. These conclusions cannot be transferred to the behavior of the clusters with respect to band bending.

DISCUSSION

The formation and growth of Si clusters on the C₆₀ surface has been observed and a description of the progression of the cluster growth and the interaction between the two materials can now be developed. The modification of the Si-signal intensity as a function of the nominal coverage confirms the cluster growth mode and nonwetting behavior of Si. From the C1s core level it can be concluded that the adsorption of Si atoms does not lead to the formation of covalently bonded SiC and the fullerene cages remain intact during the experiment. An earlier study on the formation of Si-C₆₀ composite materials showed that for the breaking of the carbon cages and reaction with the surrounding Si matrix to form SiC temperatures exceeding 970 K are required.³⁵

The corrugation of the C₆₀ surface is considerable, due to the large size of the molecules (diameter approximately 1 nm) and relatively large interstitial vacancies are present which appear as troughs on the surface. This spatial inhomogeneity leads to the presence of a variety of adsorption sites, distinguished by the number of carbon neighbor atoms (in or outside the interstitials) and the local symmetry which can either be a hexagonal or pentagonal face of the fullerene cage. Although it is not possible from our experiment to identify the primary adsorption site, the analysis of the core levels gives some information on the preferential nucleation site for the clusters in the early stages of the deposition process. In particular the analysis of the Si2p core level offers a wealth of information. The evolution of the peak shape with increasing nominal Si coverages indicates that the cluster growth process does not proceed via Ostwald ripening where the mean cluster size increases continuously at the expense of the smaller clusters.

As can be seen in Fig. 3 the high-binding energy component to the Si2p core level dominates at very low coverages, but its concentration defined as contribution to the Si2p peak, decreases rapidly with increasing coverage. The absolute intensity on the other hand remains unchanged after the first two deposition steps. Binding energy difference Δ is independent of the cluster size and this component is tentatively assigned to Si atoms residing in a predominantly carbon environment, which is present in the interstitials between the fullerene molecules. In general, Si atoms surrounded by carbon atoms will be found at higher binding energies than those with solely Si neighbors (binding energy for SiC 100.4 eV and for Si 99.4 eV).³⁵ A simple geometrical consideration shows that only a few Si atoms can occupy the interstitials and be in contact with the C₆₀ molecules. The amount of Si atoms which has to be deposited to fill the interstitials (about 3–4 atoms per interstitial if they have predominantly carbon neighbors) corresponds to the amount which was deposited when the slope in the Si2p peak position started to level off (0.03–0.04 nm nominal Si coverage)

and the concentration of the high-binding energy contribution becomes very small. Increasing the Si concentration at the surface leads to the formation of more and more clusters where Si atoms with predominantly Si neighbors are present, which contribute to the low-binding energy component. After the formation of these very small clusters in the interstitials the cluster growth continues as more Si is deposited on the surface and the Si-Si bonding environment begins to dominate. The larger half width and slightly increased asymmetry of the low-binding energy component are commensurate with a larger range of bonding environments, and the presence of a variety of cluster sizes and shapes. The peak position is strongly dependent on cluster size which is due to initial and final state effects which influence the photoemission process.

Due to the large excitation cross section of C_{60} in the UPS spectra as compared to Si no information on the band structure and density of states of the Si clusters can be obtained in this experiment. Future investigations will employ synchrotron radiation which allows to vary the photon energy and thus change the weight of the respective cross sections. Both, the UPS-VB spectra and the core levels were used to determine the valence band offset at the interface.

The results of this investigation support the model that the growth of Si clusters on the highly corrugated C_{60} surface begins in the interstitials between the C_{60} molecules. The first small clusters form there and might serve as nucleation centers for the subsequent cluster growth. The fullerene surface functions as a template for this process and can most likely be used to create regular cluster arrays. These findings are supported by recent theoretical work by Marcos *et al.*¹⁶ which indicates that the stability and shape of Si clusters in contact with a C_{60} molecule strongly depend on the size of the Si cluster. For cluster made of 5 or fewer atoms the bonding to the C_{60} molecule is preferred over bonding to other Si atoms, for larger clusters the trend is reversed and Si—Si bonds are more favorable and stabilize the clusters. Interestingly recent experiments in our group with Au as adatoms indicate no preferential nucleation sites for this materials combination. Future experiments investigating the (local) electronic structure and topography with scanning probe methods and photoelectron spectroscopy with different photon energies to promote emission from the Si clusters will

help to clarify this picture. The C_{60} can function as a template for the formation of regular cluster arrays (superstructures) of Si which can easily be expanded to 3D by sequential deposition or possibly codeposition of C_{60} and Si. The 2D arrays could be exploited as “docking” points for organic molecules, creating stable arrays for sensing or similar applications. A considerable advantage for this type of applications is the ease of deposition of the C_{60} surface as a template.

CONCLUSIONS

The deposition of Si on the highly corrugated C_{60} surface proceeds via cluster growth mode and presents a system where the cluster nucleation is closely tied to the surface structure. The photoelectron spectroscopy observation of the deposition process was combined with a numerical fit procedure applied in the analysis of the core levels and allowed us to distinguish between different bonding sites. The high carbon coordination site is preferred early in the deposition process, the interstitials in the C_{60} surface are apparently the preferred nucleation sites. In these sites the number of carbon neighbors is maximized, in accordance with Marcos *et al.*¹⁶ who predicted this to be the preferred environment for small Si clusters with less than five atoms. As the cluster growth proceeds the Si bonding environment gains in importance and the intensity of the corresponding Si2*p* peak rapidly increases. The absence of a SiC component in the C1*s* spectra excludes a substitutional doping of the fullerene cage with Si. The C_{60} can function as a template for the formation of regular cluster arrays (superstructures) of Si clusters and an expansion to three dimensional structures is possible.

From the XPS and UPS spectra the valence band offset at the interface of the resultant *a*-Si- C_{60} heterostructure has been determined and amounts to 1.2 eV. The UPS-VB spectra confirm the absence of a charge transfer or directed covalent bonding between the Si adsorbate and the fullerene surface. A certain degree of hybridization between Si and C_{60} due to overlap between the Si cluster and C_{60} MOs agrees with the UPS-VB spectra and does not necessarily lead to the appearance of new peaks but can be hidden in a slight peak broadening and loss of MO degeneracy.

¹M. S. Dresselhaus, G. Dresselhaus, and P. C. Eklund, *Science of Fullerenes and Carbon Nanotubes* (Academic Press, San Diego, 1996).

²D. Tomanek, Y. Wang, and R. S. Ruoff, *J. Phys. Chem. Solids* **12**, 1679 (1993).

³H. Shinohara, *Rep. Prog. Phys.* **63**, 843 (2000).

⁴Y. Wang, D. Tomanek, G. F. Bertsch, and R. S. Ruoff, *Phys. Rev. B* **47**, 6711 (1993).

⁵T. Yildirim, O. Zhou, J. E. Fischer, N. Bykovetz, R. A. Strongin, M. A. Cichy, A. B. Smith, III, C. L. Lin, and R. Jelinek, *Nature (London)* **360**, 568 (1992).

⁶O. Gunnarsson, *Rev. Mod. Phys.* **69**, 575 (1997).

⁷T. R. Ohno, Y. Chen, S. E. Harvey, G. H. Kroll, P. J. Benning, J. H. Weaver, L. P. F. Chibante, and R. E. Smalley, *Phys. Rev. B* **47**, 2389 (1993).

⁸C. Gu, F. Stepniak, D. M. Poirier, M. B. Jost, P. J. Benning, Y. Chen, T. R. Ohno, J. L. Martins, J. Fure, and R. E. Smalley, *Phys. Rev. B* **45**, 6348 (1992).

⁹Y. Chen, F. Stepniak, J. H. Weaver, L. P. F. Chibante, and R. E. Smalley, *Phys. Rev. B* **45**, 8845 (1992).

¹⁰T. R. Ohno, G. H. Kroll, J. H. Weaver, L. P. F. Chibante, and R. E. Smalley, *Phys. Rev. B* **46**, 10 437 (1992).

¹¹L. Qian, L. Norin, J.-H. Guo, C. Sathe, A. Agui, U. Jansson, and J. Nordgren, *Phys. Rev. B* **59**, 12 667 (1999).

- ¹²A. V. Talyzin, H. Högberg, and U. Jansson, *Thin Solid Films* **405**, 42 (2002).
- ¹³A. V. Talyzin and U. Jansson, *Thin Solid Films* **429**, 96 (2003).
- ¹⁴D. Klyachko and D. M. Chen, *J. Vac. Sci. Technol. B* **15**, 1295 (1997).
- ¹⁵B. Massenelli, F. Tournus, P. Melinon, A. Perez, and X. Blase, *J. Chem. Phys.* **117**, 10627 (2002).
- ¹⁶P. A. Marcos, J. A. Alonso, M. J. Lopez, and E. Hernandez, *Compos. Sci. Technol.* **63**, 1499 (2003).
- ¹⁷B. Massenelli, F. Tournus, P. Melinon, X. Blase, A. Perez, M. Pellarin, and M. Broyer, *Appl. Surf. Sci.* **226**, 226 (2004).
- ¹⁸P. Reinke, P. Oelhafen, and S. Christiansen, *Surf. Sci.* **507**, 630 (2002).
- ¹⁹F. Tournus, B. Massenelli, P. Melinon, X. Blase, A. Perez, M. Pellarin, M. Broyer, A. M. Flank, and P. Lagarde, *Phys. Rev. B* **65**, 165417 (2002).
- ²⁰O. Janzen and W. Mönch, *J. Phys.: Condens. Matter* **11**, L111 (1999).
- ²¹D. Kondo, K. Sakamoto, H. Takeda, F. Matsui, K. Amemiya, T. Ohta, W. Uchida, and A. Kasuya, *Surf. Sci.* **514**, 337 (2002).
- ²²K. Sakamoto, D. Kondo, M. Harada, A. Kimura, A. Kakizaki, and S. Suto, *Surf. Sci.* **433**, 642 (1999).
- ²³K. Sakamoto, D. Kondo, H. Takeda, T. Sato, S. Suga, F. Matsui, K. Amemiya, T. Ohta, W. Uchida, and A. Kasuya, *Surf. Sci.* **493**, 604 (2001).
- ²⁴D. Sanvitto, M. De Seta, and F. Evangelisti, *Surf. Sci.* **452**, 191 (2000).
- ²⁵M. De Seta, D. Sanvitto, and F. Evangelisti, *Phys. Rev. B* **59**, 9878 (1999).
- ²⁶J. J. Yeh and I. Lindau, *At. Data Nucl. Data Tables* **32**, 1 (1985).
- ²⁷D. W. Marquard, *J. Soc. Ind. Appl. Math.* **11**, 431 (1963).
- ²⁸S. Doniach and M. Sunjic, *J. Phys. C* **3**, 285 (1970).
- ²⁹D. A. Shirley, *Phys. Rev. B* **5**, 4709 (1972).
- ³⁰S. Huefner, *Photoelectron Spectroscopy* (Springer-Verlag, Berlin, 2003).
- ³¹P. Reinke, H. Feldermann, and P. Oelhafen, *J. Chem. Phys.* **119**, 12547 (2003).
- ³²P. Rudolf, M. S. Golden, and P. A. Brühwiler, *J. Electron Spectrosc. Relat. Phenom.* **100**, 409 (1999).
- ³³S. Suto, K. Sakamoto, T. Wakita, M. Harada, and A. Kasuya, *Surf. Sci.* **402-404**, 523 (1998).
- ³⁴S. Suto, K. Sakamoto, D. Kondo, T. Wakita, A. Kimura, and A. Kakizaki, *Surf. Sci.* **427-428**, 85 (1999).
- ³⁵P. Reinke, D. Rudman, and P. Oelhafen, *Phys. Rev. B* **61**, 16 967 (2000).
- ³⁶P. J. Benning, D. M. Poirier, N. Troullier, J. L. Martins, J. H. Weaver, R. E. Haufler, L. P. F. Chibante, and R. E. Smalley, *Phys. Rev. B* **44**, 1962 (1991).
- ³⁷N. Troullier and J. L. Martins, *Phys. Rev. B* **46**, 1754 (1992).
- ³⁸W. L. Yang, V. Brouet, X. J. Zhou, H. J. Choi, A. G. Louie, M. L. Cohen, S. A. Kellar, P. V. Bogdanov, A. Lanzara, A. Goldoni, F. Parmigiani, Z. Hussain, and Z.-X. Shen, *Science* **300**, 303 (2003).
- ³⁹P. Reinke and P. Oelhafen, *J. Chem. Phys.* **116**, 9850 (2002).
- ⁴⁰G. K. Wertheim and S. B. DiCenzo, *Phys. Rev. B* **37**, 844 (1988).
- ⁴¹G. K. Wertheim, S. B. DiCenzo, and S. E. Youngquist, *Phys. Rev. Lett.* **51**, 2310 (1983).
- ⁴²K. H. Meiwes-Broer, *Metal Clusters at Surfaces* (Springer-Verlag, Berlin, 2000).
- ⁴³H. Hövel, B. Grimm, M. Pollmann, and B. Reihl, *Phys. Rev. Lett.* **81**, 4608 (1998).
- ⁴⁴G. Gensterblum, K. Hevesi, B.-Y. Han, L.-M. Yu, J.-J. Pireaux, P. A. Thiry, D. Bernaerts, S. Amelinckx, G. Vantendeloo, G. Bendele, T. Buslaps, R. L. Johnson, M. Foss, R. Feigenhans'l, and G. L. Lay, *Phys. Rev. B* **50**, 11 981 (1994).
- ⁴⁵R. W. Lof, M. A. v. Veenendaal, B. Koopmans, H. T. Jonkman, and G. A. Sawatzky, *Phys. Rev. Lett.* **68**, 3924 (1992).
- ⁴⁶S. Saito and A. Oshiyama, *Phys. Rev. B* **44**, 11 532 (1991).
- ⁴⁷J. Onoe, A. Nakao, and K. Takeuchi, *Phys. Rev. B* **55**, 10 051 (1997).
- ⁴⁸E. A. Kraut, R. W. Grant, J. R. Waldrop, and S. P. Kowalczyk, *Phys. Rev. Lett.* **44**, 1620 (1980).